Lightning-produced NOx in an explicit electrical scheme tested in a Stratosphere-Troposphere Experiment : Radiation, Aerosols, and Ozone case study.

Christelle Barthe, Jean-Pierre Pinty, C. Mari

Lightning-produced NO_x in an explicit electrical scheme tested in a Stratosphere-Troposphere Experiment: Radiation, Aerosols, and Ozone case study

Christelle Barthe,[1] Jean-Pierre Pinty,[1] and Céline Mari[1]

Received 13 April 2006; revised 1 September 2006; accepted 5 October 2006; published 21 February 2007.

[1] An explicit lightning-produced nitrogen oxide (LNO_x) scheme has been implemented in a 3-D mesoscale model. The scheme is based on the simulation of the electrical state of the cloud and provides a prediction of the temporal and spatial distribution of the lightning flashes. The frequency and the 3-D morphology of the lightning flashes are captured realistically so fresh nitrogen oxide molecules can be added along the complex flash path as a function of the pressure, as suggested by results from laboratory experiments. The scheme is tested on the 10 July 1996 Stratosphere-Troposphere Experiment: Radiation, Aerosols, and Ozone (STERAO) storm. The model reproduces many features of the observed increase of electrical activity and LNO_x flux density between the multicell and supercell stages. LNO_x dominates the NO_x budget in the upper part of the cells with instantaneous peak concentrations exceeding 4 ppbv, as observed. The computed flux of NO_x across the anvil shows a mean value of 6 mol m^{-2} s^{-1} during the last 90 min of the simulation. This value is remarkably stable and compares favorably with the observations.

Citation: Barthe, C., J.-P. Pinty, and C. Mari (2007), Lightning-produced NO_x in an explicit electrical scheme tested in a Stratosphere-Troposphere Experiment: Radiation, Aerosols, and Ozone case study, *J. Geophys. Res.*, *112*, D04302, doi:10.1029/2006JD007402.

1. Introduction

[2] Nitrogen oxides ($NO_x \equiv NO + NO_2$) are important trace gases in the atmosphere since they are precursors of tropospheric ozone. They control the photochemical regimes of the troposphere and the hydroxyl radical concentration which is the main oxidant of numerous chemical species. NO_x also has an influence in the stratosphere where it reacts with the odd oxygen in the ozone layer.

[3] Lightning flashes are considered to be a major natural source of the NO_x budget. Lightning-produced NO_x (LNO_x) is directly available in the upper troposphere where its lifetime is large compared to lower altitudes. However, a large uncertainty exists in LNO_x production at the global scale where the estimates range from 2 to 20 Tg(N) yr^{-1} [*Lee et al.*, 1997]. This is partly due to the complexity of deep convective processes in the tropics, but also to the incomplete understanding of the physical processes related to the separation of the electric charges, the triggering of lightning flashes and finally the LNO_x production at storm scale.

[4] In global models, LNO_x production relies on a parameterization of the lightning activity and assumes a bulk vertical distribution. The often used parameterization of *Price and Rind* [1992] calculates the flash frequency as a power function of cloud top height. Other parameterizations are based on the vertical mass flux [*Allen and Pickering*, 2002], on the convective precipitation [*Meijer et al.*, 2000] or on the convective available potential energy [*Choi et al.*, 2005]. In retrospect, it is the excessive LNO_x sensitivity to these poorly constrained electrical proxies [*Choi et al.*, 2005] that motivates the present work.

[5] An avenue for improved modeling of the global LNO_x source is through cloud resolving models (CRM) with explicit three-dimensional representation of the dynamics and microphysics of the storms and of their electrical properties. So far just a few CRM-based electrification studies have been undertaken [*Helsdon and Farley*, 1987; *Helsdon et al.*, 1992; *Mansell et al.*, 2002; *Barthe et al.*, 2005; *Altaratz et al.*, 2005]. Among these, only the first three models are potentially able to model LNO_x production given the predicted electrical state of deep convective clouds. This is testimony to the difficulty of devising, setting up and testing a true lightning scheme that can reproduce both the frequency and the spatial extent of lightning flashes associated with the distribution of electrical charges and of the electric field in deep convection events.

[6] The purpose of this study is to demonstrate that a LNO_x production can be reasonably well simulated with an explicit electrical scheme [*Barthe et al.*, 2005] once coupled to a laboratory calibrated NO production per discharge length [*Wang et al.*, 1998] in a 3-D mesoscale model. We first show why previous lightning parameterizations fail or seem not well suited to predict the spatial and the temporal

[1]Laboratoire d'Aérologie, Université Paul Sabatier and Centre National de la Recherche Scientifique, Toulouse, France.

0148-0227/07/2006JD007402

location of the LNO_x sources. Then we present the flash scheme and the associated LNO_x production. Finally, we illustrate the method using the well-documented observations of the 10 July 1996 Stratospheric-Tropospheric Experiment: Radiation, Aerosols, and Ozone (STERAO) storm [*Dye et al.*, 2000]. The simulated electrical state of the storm is discussed. We show that the evolving lightning activity is partially related to the development stage of the storm. As a result the NO_x budget varies in time as illustrated by the estimation of NO_x flux across storm anvil.

2. Lightning-Produced NO_x in Cloud Resolving Models

[7] A few mesoscale models include a parameterization of LNO_x production to study convective transport and chemical transformations at the regional scale. *Pickering et al.* [1998] were the first to construct a highly parameterized LNO_x production in a 2-D/3-D CRM based on *Price and Rind* [1992]. The LNO_x source follows *Price et al.* [1997] with a horizontally uniform vertical distribution of NO_x in areas where the radar reflectivity is higher than 20 dBZ but the temperature is less than $-15°C$ for the placement of cloud-to-ground (CG) flashes. It is assumed that intracloud (IC) flashes prevail in cloudy areas above the $-15°C$ isotherm. The parameterization of *Pickering et al.* [1998] is based on statistically calibrated flash rate, flash type and LNO_x per flash rate. The flash rate is a function of the peak updraft. This parameterization is easy to implement too and *Fehr et al.* [2004] adapted it with modifications to simulate a LNO_x production in a EULINOX (European Lightning Nitrogen Oxides Experiment) storm. However such a crude parameterizations do not reproduce the physics of the discharges, so they must be done cautiously when studying LNO_x emissions by individual storms. For instance, in contrast with *Price et al.* [1997], a recent review [*Ridley et al.*, 2005] concludes that observations, theory and modeling work suggest that IC and CG flashes probably produce a similar quantity of NO molecules per flash. Modeling studies of *DeCaria et al.* [2005] confirmed the conclusions of *Ridley et al.* [2005].

[8] *DeCaria et al.* [2000, 2005] modified *Pickering et al.* [1998] by introducing Gaussian distributions to create distinct NO_x vertical modes. They reconsidered the area where IC and CG flashes might propagate according to *MacGorman et al.* [1981]. They introduced a vertical distribution function for lightning segments. However their original scheme is not fully predictive since the lightning flash frequency is constrained by the observations and furthermore their NO_x production efficiency by IC and CG flashes is an adjustable parameter.

[9] An attempt at a more physically sound approach of LNO_x production at storm scale was made by *Wang and Prinn* [2000], but *Helsdon* [2004] argued that such a simplified geometrical model of electric charge distribution may dramatically underestimate the flash rate. Moreover, the fixed CG/IC ratio and the supposedly enhanced efficiency of the CG flashes remain also questionable for a realistic production of LNO_x by the scheme.

[10] *Zhang et al.* [2003a] first introduced a LNO_x parameterization in a CRM which was based on an explicit and complete electrical scheme [*Helsdon et al.*, 1992]. Here the lightning flash consists of a quasi-vertical channel which propagates along the electric field according to the model of *Kasemir* [1960, 1983]. The lightning channel is surrounded by a volumic halo where uniformly distributed LNO_x molecules are introduced in proportion to the dissipated energy and to the electrical charge. CG flashes are not simulated. Although discharges and hence puffs of LNO_x are produced in response to a truly simulated electrical state, the lightning scheme leads to a single, unbranched channel that does not include extended IC lightning paths of several tens of km far away from the origin of the initial breakdown. Furthermore a first three-dimensional simulation on a reduced domain ($50 \times 50 \times 40$ grid points) with a doubled linear capacitance of the original lightning scheme [*Zhang et al.*, 2003b] was shown to produce just a few concentrated lightning events (18 IC during a 3-min period only). Although *Zhang et al.* [2003b] claim that their simulation is in agreement with various field measurements, no comparison with data of highly electrically active storms has been performed up to now. The model predicted production of lightning flash rate for the CCOPE storm was much less than flash rates observed in other midlatitude, continental convection [*Defer et al.*, 2001; *Fehr et al.*, 2004].

[11] The deficiency and uncertainties of the above studies come from their poor or rudimentary ability to describe the sporadic and branching characteristics of lightning events that lead to LNO_x bursts. As illustrated in Figure 1 for a selected STERAO leg, the airborne NO signal clearly depicts the convective outflow with a mean 1 ppbv concentration of NO well above a nearly zero background level. The sharp peaks of NO in Figure 1 (e.g., 4 ppbv at 2308 UTC) are a fascinating feature that *Stith et al.* [1999] showed to be associated with the sampling of fresh LNO_x before dilution. Given these sharp features, it seems worthwhile to explore a LNO_x production rate based on short segments forming the lightning channels. Our goal is to give a detailed description of the LNO_x source strengths and locations so that we can derive a more accurate budget of NO in deep convective clouds. As suggested by *Zhang et al.* [2003a], it seems difficult to simulate a flash to flash variability and hence a timely and accurate LNO_x production without the support of an electrical scheme. The purpose of this study is to explore this idea, but with an original lightning scheme [*Barthe et al.*, 2005] and with a more consistent LNO_x production parameterization that fully exploits the characteristics of the simulated lightning flashes.

3. Model Description

[12] The LNO_x parameterization has been developed in the mesoscale model Meso-NH [*Lafore et al.*, 1998]. The model has a complete electrification and lightning flash scheme described in *Barthe et al.* [2005]. The electric charges are carried by each of the five hydrometeor categories of the mixed phase microphysical scheme. They are mostly separated by elastic ice-graupel collisions, known as a noninductive process. The charges are transported and transferred between hydrometeors following, but not necessarily in proportion of microphysical mass transfer rates (see *Barthe et al.* [2005] for details). The electric field is obtained by integrating a Poisson equation involving net

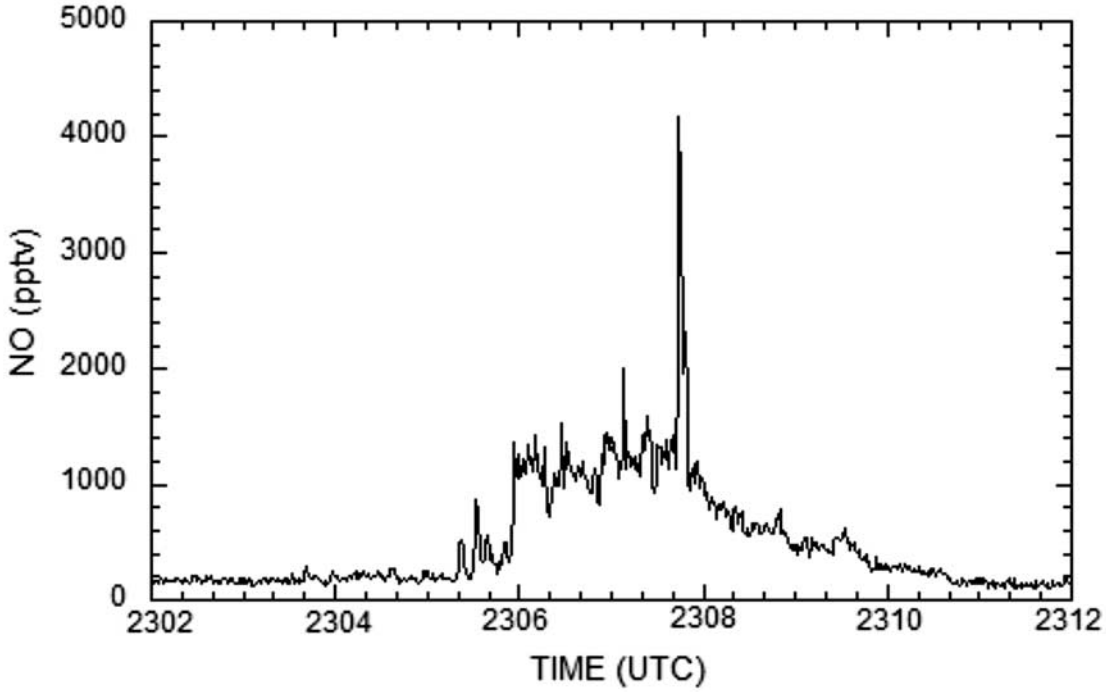

Figure 1. NO concentrations measured by the Citation at 11.6 km msl from 2305 to 2311 UTC, approximately 10–15 km downwind of the convective core. (Redrawn with courtesy by J. Dye from *Dye et al.* [2000].)

charge densities and appropriate boundary conditions. The lightning flash scheme consists of two parts: a quasi-vertical bidirectional leader and growing branching streamers. The leader is triggered and propagates according to the ambient electric field. Branches are generated by an iterative algorithm. The maximum number of branches at a given distance from the initiation point obeys a fractal law as suggested from dielectric breakdown model results. The scheme mimics branches and especially the horizontal extension of IC flashes. This approach is pragmatic and leads to the formation of realistic lightning flash paths similar to the complex structures observed by recent detection systems [*Rison et al.*, 1999] and that emerge from dielectric breakdown models as shown by *Mansell et al.* [2002].

[13] As the lightning flash scheme in Meso-NH reproduces the lightning flash path and tortuosity, it is interesting to investigate the dependance of the LNO_x production with the flash length. Thus, in the model, the LNO_x production is taken proportional to the lightning flash length and depends on the atmospheric pressure [*Wang et al.*, 1998]:

$$n_{NO}(P) = a + bP \tag{1}$$

with $a = 0.34\ 10^{21}$, $b = 1.30\ 10^{16}$. P is the pressure in Pa, and n_{NO} is the amount of NO produced per unit length (in molecules m^{-1}). Mean segment lengths are computed and a LNO_x mass is added to the grid points of the lightning path. Equation (1) is especially well suited to lightning schemes that rely on a detailed description of the filamentary aspect of lightning flashes. No attempt was made to modify the original calibration of the a and b coefficients.

[14] No chemistry is considered in the present study to simplify the analysis. The impact of the LNO_x source is evaluated by comparing two tracers that simulate NO with and without the LNO_x source.

4. Simulation of the 10 July 1996 STERAO Storm

4.1. Model Initialization and First Results

[15] Convection is initiated by three warm bubbles (+1°C) along the wind axis in the manner described by *Skamarock et al.* [2000]. The computational domain is 160 × 160 × 50 grid points with a constant horizontal grid spacing of 1 km and a vertical spacing of 75 m at the ground stretching to 700 m in the stratosphere. The initial sounding comes from *Skamarock et al.* [2000], and the initial NO profile is taken from *Skamarock et al.* [2003] (see Figure 2). Lateral boundary conditions are open, and an upper sponge layer is used to attenuate the reflection of gravity waves by the rigid lid at 23,000 m. Only noninductive processes [*Takahashi*, 1978] are allowed to electrify the cloud. The 3-D turbulence scheme of *Cuxart et al.* [2000] is used.

[16] The 10 July 1996 storm was initially multicellular but evolved to a supercellular storm after 2 hours [*Dye et al.*, 2000; *Skamarock et al.*, 2000]. The Meso-NH model captures the storm transition from multicellular to supercellular characteristics as seen with dynamical and electrical diagnostics as shown in Figure 3. Figure 3 (top) presents the upward/downward peak velocities, $w_{\max}^{up}$ and $w_{\max}^{down}$. The multicell stage in the model is characterized by moderate to high vertical velocities ($w_{\max}^{up} \sim 25$ m s^{-1} and $w_{\max}^{down} \sim -7.5$ m s^{-1}) while very intense motions ($w_{\max}^{up} > 40$ m s^{-1} and $w_{\max}^{down} < -20$ m s^{-1}) are found near the beginning of the supercell stage and also at about 200 min into the simula-

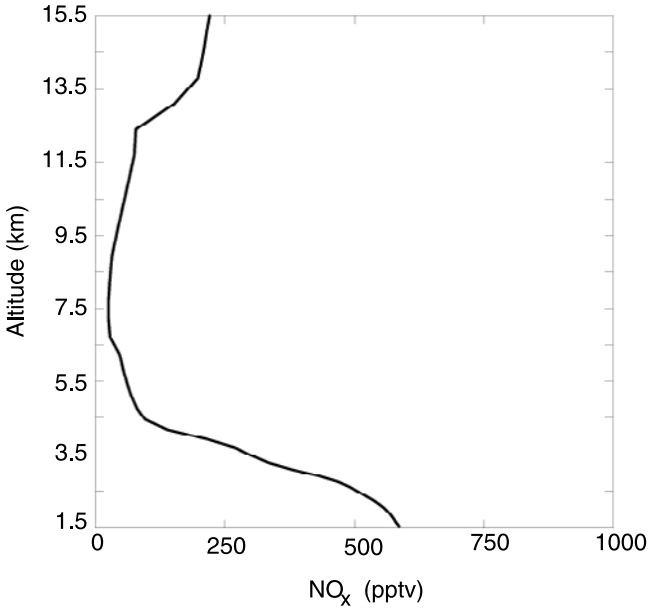

Figure 2. Environmental profile of NO_x used in the simulation and taken from *Skamarock et al.* [2003].

tion. Toward the end of the simulation period updrafts and downdrafts gradually increase to large values. In reality, infrared satellite pictures (not shown here) reveal that the storm was beginning to decay well after ~300 min.

[17] As seen in Figure 3 (bottom), each convective stage is characterized by distinct regimes of electrical activity. At the beginning of the multicellular stage, the flash rate is around 5–12 flashes min^{-1}, followed by a peak at 30 flashes min^{-1} while *Defer et al.* [2001] estimated the maximum flash rate to 50 flashes min^{-1}. It is worth noting that the maximum flash rate in *Defer et al.* [2001] and *Skamarock et al.* [2003] differs as a result of different averaging periods. As in the observations, the flash rate rapidly decreases at the end of the multicellular stage. About 10–30 flashes min^{-1} were observed during the transition stage, but none is reproduced by the model for a period of 80 min. This is attributed to a lack of supercooled liquid water in the convective cells which restricts the charging process (as detailed later in Figure 8 in section 4.3). Then the electrical activity becomes again very intense in the supercellular stage. In the model, between 12.5 and 30 flashes min^{-1} are triggered during 20 min and two peaks at 40 flashes min^{-1} are recorded. Observations show a sustained lightning flash activity during 60 min with up to 60 flashes min^{-1}. Then residual electrified cells last up to the end of the simulation. *Defer et al.* [2001] reported the detection of 5428 flashes during this 10 July 1996 STERAO storm but with 50% short-duration flashes having length shorter than 1 km [see *Defer et al.*, 2003]. 2048 flashes are triggered with Meso-NH, but the model is not able to simulate short-duration flashes. The number of lightning flashes seems underestimated by the model, but considering the known uncertainties of the electrification scheme, we conclude that the simulated flash frequency is acceptable for examining the LNO_x production. This analysis is supported by the large proportion of observed short-duration pulses [*Defer et al.*, 2003] which probably contribute much less, if any, to the LNO_x budget. The electric field in the model is well constrained as the maximum electric field is always less than 200 kV m^{-1} (Figure 3) in agreement with *Marshall et al.* [1995].

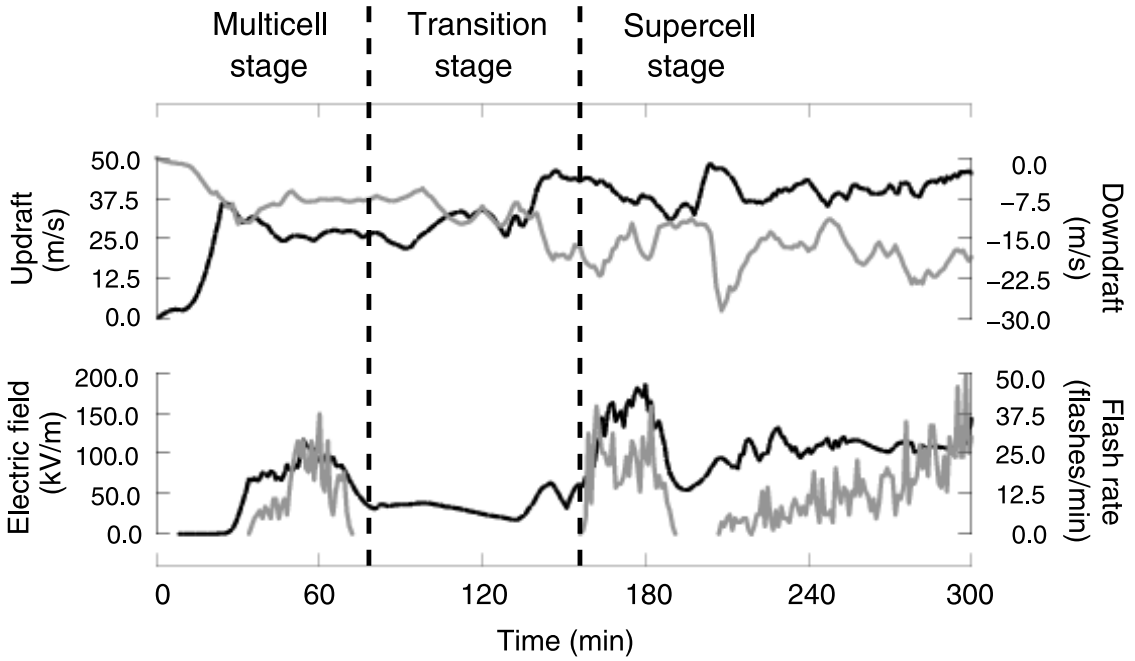

Figure 3. Time series (top) of the simulated maximum updraft (solid line) and downdraft (shaded line) and (bottom) of the simulated maximum electric field in kV m^{-1} (solid line) and lightning flash frequency in number of flashes per minute (shaded line). The different regimes of the storm are depicted by the vertical dashed lines.

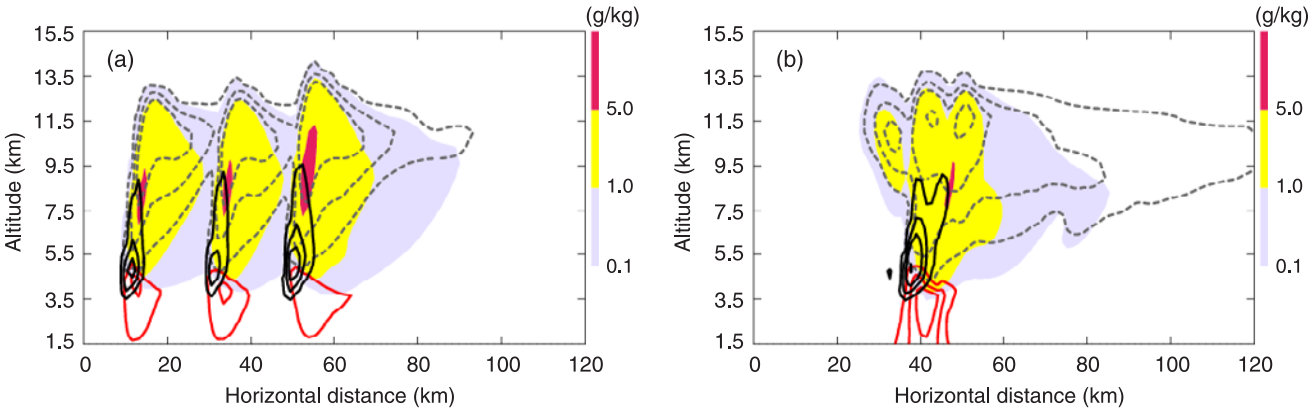

Figure 4. Partial vertical along-wind cross section at (a) 1 hour and (b) 2.5 hours of the hydrometeor mixing ratios. Colored areas, gray dashed lines, black solid lines and red solid lines represent graupel, pristine ice and snow, cloud droplet and rain drop mixing ratios respectively. The mixing ratio contours are 0.1, 0.5, 1 and 2 g kg^{-1} for pristine ice and snow, cloud droplets and rain drops.

[18] Figure 4 shows vertical cross sections of hydrometeor mixing ratios at 1 hour and 2.5 hours. During the multicellular stage (Figure 4a), three aligned convective cells are in a NW-SE direction. Each cell reaches 13.5 km altitude and has an horizontal extension of 20 km. The central cell contains a low cloud droplet mixing ratio ($r_c \sim 0.5$ g kg^{-1}) compared to that of the two outer cells ($r_c > 1$ g kg^{-1}). In the central cell, the rain mixing ratio reaches 0.6 g kg^{-1}, while in the northwestern cell and in the southeastern cell, the rain mixing ratio is 0.5 and 0.4 g kg^{-1} respectively. The pristine ice and snow mixing ratio is higher in the southeastern cell ($r_i \sim 2$ g kg^{-1}) than in the two other cells ($r_c \sim 1.5$ g kg^{-1}). In the same vein, the graupel mixing ratio reaches higher values in the downwind cell. Therefore, in the central cell with a lower vertical velocity (not shown here), precipitation is generated by warm processes, while in the two other cells, cold processes dominate the precipitation formation. The low liquid water content associated with the low graupel and ice mixing ratio in the central cell would lead to a less electrical efficiency in this cell, and therefore to a lower production of LNO_x. During the supercellular stage (Figure 4b), the anvil extends on 100 km in the NW-SE direction. At 11.5 km altitude, the pristine ice and snow mixing ratio reaches 2 g kg^{-1}. The maximum graupel mixing ratio remains around 5 g kg^{-1} at 8 km. The cloud droplet and the rain drop mixing ratios increase and reach 2 g kg^{-1} and 1.5 g kg^{-1} respectively.

4.2. Analysis of the LNO_x Production

[19] Figure 5 shows a vertical cross section of NO_x concentration, and of total charge density through the three multicell cores, after one hour of simulation. Each cell is characterized by an inverted bipolar distribution of negative (upper part) and positive (lower part) charges. This structure is quite different from the classical tripolar structure [*Williams*, 1989] or from the highly stratified structure discussed by *Stolzenburg et al.* [1998]. However such an electrical structure was observed by *Rust and MacGorman* [2002] during the STEPS campaign. The negative charge density reaches -0.4 nC m^{-3} in the first cell while it does not exceed -0.1 nC m^{-3} in the central cell. This cell is less electrified as a result of a low liquid water content (shown in Figure 4a, and also detectable in the work by *Skamarock et al.* [2000, Figure 8]). In reality, the central cell is more efficient at producing early precipitating drops by warm microphysical processes in the low levels. Less water is then available for the ice-graupel charging process according to the parameterization of *Takahashi* [1978]. In Figure 5, the NO_x field is dominated by the LNO_x contribution in the 7500–13,500 m layer of the two external cells. The instantaneous NO_x peak value is 6.2 ppbv, well above the 0.5 ppbv level transported from the top of the boundary layer. This is consistent with Figure 1 that shows NO concentrations measured by the Citation at 11.6 km altitude during the multicellular stage. From 2302 to 2305 UTC, the NO

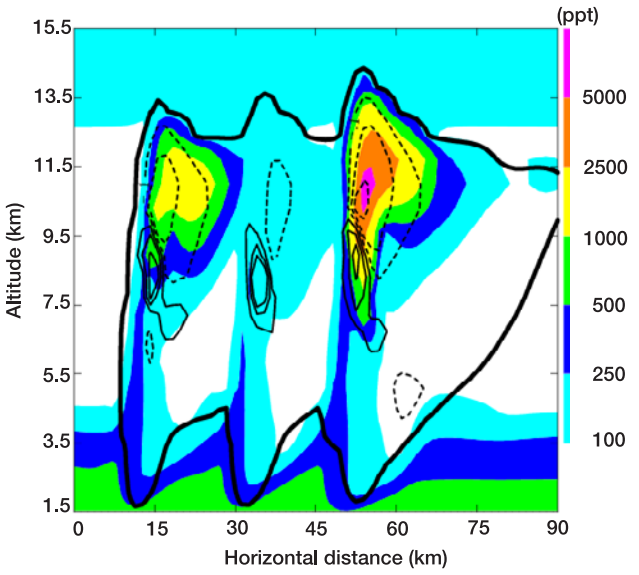

Figure 5. Along-wind vertical cross section at 1 hour of the NO_x concentration (colored areas in pptv) and of the total electric charge density (thin lines). The charge density contours are ±0.1, ±0.3 and ±0.5 nC m^{-3} (negative values are dashed). The cloud limit is outlined (thick solid line).

Table 1. Airborne Measurements of NO Peak Values in Recent Field Experiments

Reference	Experiment	NO Peak Value
Huntrieser et al. [1998]	LINOX	4.0 ppbv
Stith et al. [1999]	STERAO (9 Jul)	18.7 ppbv
Dye et al. [2000]	STERAO (10 Jul)	4.2 ppbv
Lange et al. [2001]	STREAM	3.8 ppbv
Huntrieser et al. [2002]	EULINOX (3 Jul)	7.0 ppbv
Huntrieser et al. [2002]	EULINOX (17 Jul)	3.7 ppbv
Huntrieser et al. [2002]	EULINOX (21 Jul)	25.0 ppbv
Ridley et al. [2004]	CRYSTAL-FACE	9.5 ppbv

mixing ratio is about 200 pptv, which is indicative of NO transported by convection from the boundary layer. Then, between 2306 and 2310 UTC, the NO mixing ratio increases up to 1000 pptv. This value is characteristic of NO produced by flashes and diluted. A peak of NO at 4.2 ppbv appears before 2308 UTC. It is associated to fresh LNO_x before dilution [*Stith et al.*, 1999]. In Figure 5 the peak value 6.2 ppbv is located at 11 km altitude. As the Citation does not sample the LNO_x peak, the results from the Meso-NH simulation are in agreement with observations of this storm. Moreover, this peak value fits the range of upper tropospheric NO measurements taken during the various field experiments reported in Table 1. These values are only indicative because lightning flashes are triggered at random with respect to the aircraft legs. Exceptionally high values (~19 ppbv) are recorded by *Stith et al.* [1999] and by *Huntrieser et al.* [2002] with a spike of ~24 ppbv. However *Huntrieser et al.* [2002] indicated that the measurement was made in the vicinity of an artificially triggered lightning stroke that hit the research aircraft at the same time, thus suggesting that this NO_x value could be discarded. Therefore detected peak values of NO concentration are in the range of 3.7–9.5 ppbv, which is consistent with the peak value obtained with Meso-NH.

[20] To summarize, Figure 5 illustrates the double role of the deep convection: to vent the rich NO_x air of the boundary layer and to create and to transport fresh LNO_x in the mid-upper troposphere.

[21] Figure 6 shows a selected vertical cross section of the NO_x concentration after 1 hour of simulation. The cross section is taken through the anvil. Outside the cloud, the NO_x concentration is similar to the initial profile (Figure 2). High NO_x concentration is found in the boundary layer, between 1500 and 3500 m altitude Then, the NO_x concentration decreases to 25 pptv at 7500 m, and increases in the upper part of the domain. Inside the cloud, three peaks of NO_x concentration are located above 10 km altitude. They are due to the production of NO_x by lightning flashes. The left peak is centered around 10.5 km and the NO_x mixing ratio reaches 1 ppbv. The second peak is located at 11.5 km altitude and the NO_x mixing ratio is lower than in the left peak. The NO_x mixing ratio peak at 12.5 km altitude does not exceed 420 pptv. The two rightmost peaks in Figure 6 originate from the northwestern cell, while the left peak comes from the southeastern cell. Around these peaks, the NO_x mixing ratio is about 200–300 ppb. These values are probably due to the transport of NO_x from the boundary layer and to LNO_x production and dilution. Figure 6 compares reasonably will with the analyzed observations shown by *Skamarock et al.* [2003, Figure 4].

[22] The hourly LNO_x field is displayed through a series of plots in Figure 7 for three elevations: 12,500 m, 10,000 m and 7500 m. The results obtained after one hour of simulation are coincident with the maximum electrical activity detected during the multicellular stage (see Figure 3). The two cells that are producing LNO_x in Figure 5 show up at all levels. The peak values are located slightly downwind

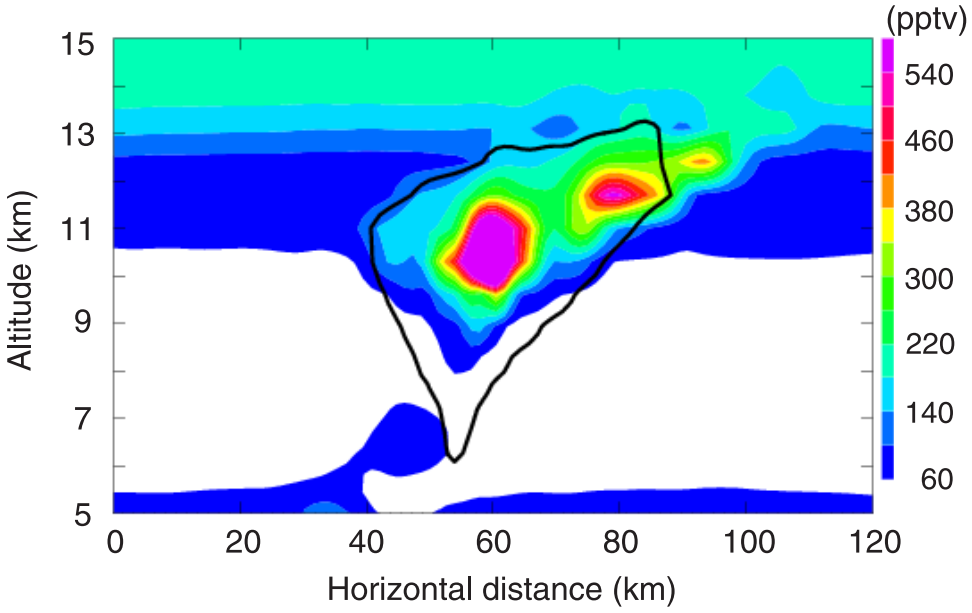

Figure 6. Vertical cross section of NO_x across the anvil in the multicellular stage. The colored areas represent the NO_x mixing ratio (in pptv), while the black solid line represents the cloud boundary. The vertical cross section at t = 1 hour corresponds to a time and position close to the Citation observations.

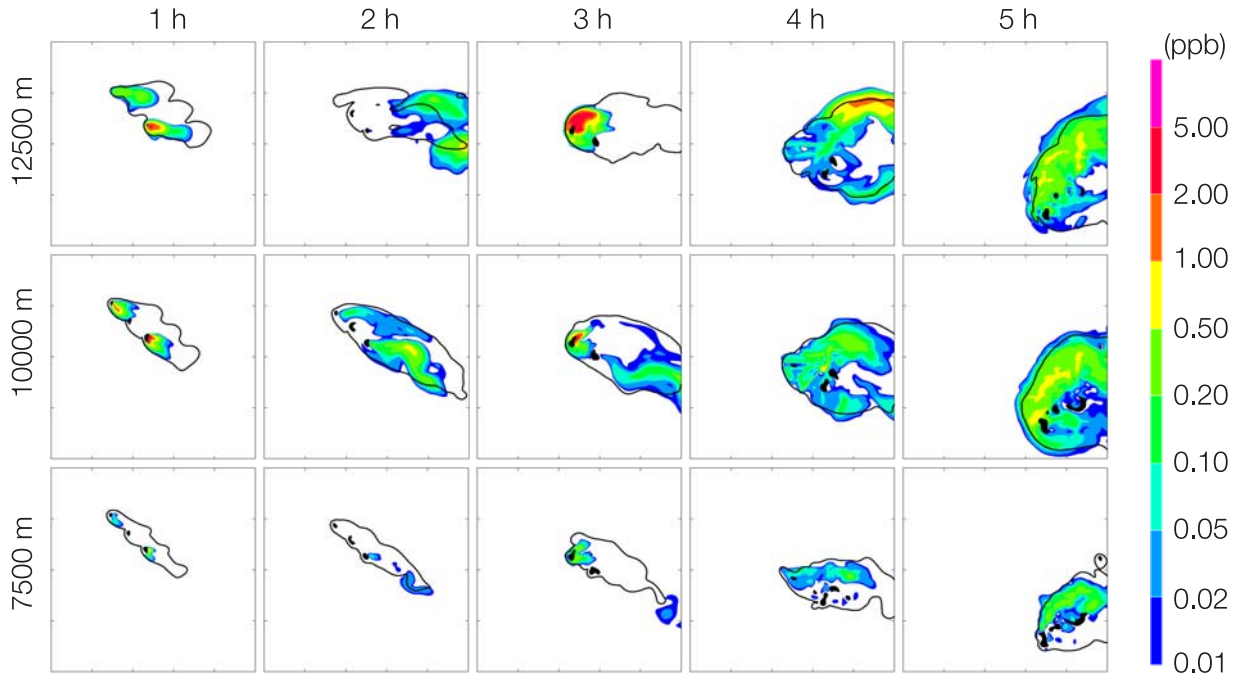

Figure 7. Horizontal cross sections at (top) 12,500 m, (middle) 10,000 m and (bottom) 7500 m of the hourly LNO_x field in logarithmic scale at 1, 2, 3, 4 and 5 hours. Areas with updrafts larger than 10 m s^{-1} are black spots. Cloud contours are outlined.

of the updrafts. At 2 hours (transition stage), the LNO_x starts to dilute and to cover a large area while moving eastward. The two puffs originating at 12,500 m maintain their identity despite the flow deformation in the wake of the cells. The LNO_x plumes appear disconnected from the updrafts as no fresh LNO_x is produced for an approximate one hour period of time. At 3 hours, the electrical supercellular stage reaches its peak and a copious amount of LNO_x appears at 12,500 m. The LNO_x production also reappears at 10,000 m as the old plume is escaping through the domain boundary. According to the flash rate trace in Figure 3, the supercell is fully developed after 4 hours but the lightning activity is moderate. Little new LNO_x is produced at 10,000 m and 7500 m. The LNO_x now fills the cloud contour at 10,000 m and above. The horseshoe shape seen at 4 hours is a result of the downwind wake of the strong updrafts. At 5 hours the large LNO_x plume reaches its full maximum expansion. The production rate of LNO_x is steady but moderate.

4.3. Fluxes and Budget of the LNO_x Production

[23] The evolution of the vertical flux profiles of LNO_x and of the cloud water mixing ratio are displayed in Figure 8. The fluxes, given in mol(NO) s^{-1} and in kg(water) s^{-1} respectively, are integrated over the domain of simulation. The vertical fluxes are defined by ρwC, where ρ is the air density, w the vertical velocity and C is the NO_x concentration or the water mixing ratio. The maxima in the LNO_x flux profiles occur at the same time as the flashes of Figure 3. These fluxes are a strong function of the vertical velocity where fresh LNO_x is created. The profiles show that the LNO_x fluxes reach an altitude 15.5 km, where they are capped by mean subsiding motion. The average tropopause height is 13.5 km approximately [*Skamarock et al.*, 2000]. Thus the 10 July STERAO case suggests that the convection was vigorous enough to detrain tropospheric air, here well enriched by LNO_x, in the lower stratosphere. This point deserves a closer look in a future study including multiphase chemistry. LNO_x fluxes are negative below 7.5 km during the last hour of simulation. This is interpreted by the presence of a substantial fraction of LNO_x in the convective downdrafts. The superimposed plot of cloud-water-mixing-ratio fluxes shows that the creation of LNO_x is delayed by roughly half an hour because of the time needed for the electrical field to grow and to become strong enough to surpass the breakdown threshold. The lack of cloud water flux explains the LNO_x flux gap during the multicell to supercell transition. This shows the important role played by a small amount of supercooled water in the storm electrical charging process.

[24] Figure 9 displays the NO_x horizontal flux density estimates (with and without flashes) through the anvil. The computation of this flux, $\langle F_h^{NO} \rangle$, is detailed in Appendix A. We prefer to estimate a mean horizontal flux because the storm-relative positioning of the Citation leg cross sections shown by *Skamarock et al.* [2003] is uncertain. The LNO_x fraction is the difference between the two curves. It follows the lightning flash frequency. The NO_x-without-LNO_x-source flux increases from 2.6 mol m^{-2} s^{-1} at 60 min to 3.8 mol m^{-2} s^{-1} at 300 min. The first flash is triggered at 34 min. The two curves diverge 15 min later showing the presence of LNO_x in the anvil. Then the two curves tend to reconnect as the LNO_x almost exits the domain at the end of the transition stage. The next supercellular stage leads to a net increase of the LNO_x flux density of ~2.8 mol m^{-2} s^{-1} after 5 hours. Note that from Figures 8 and 9, LNO_x vertical fluxes lead to an increase of the anvil fluxes following the spread of LNO_x out of the updrafts. Our results of the anvil

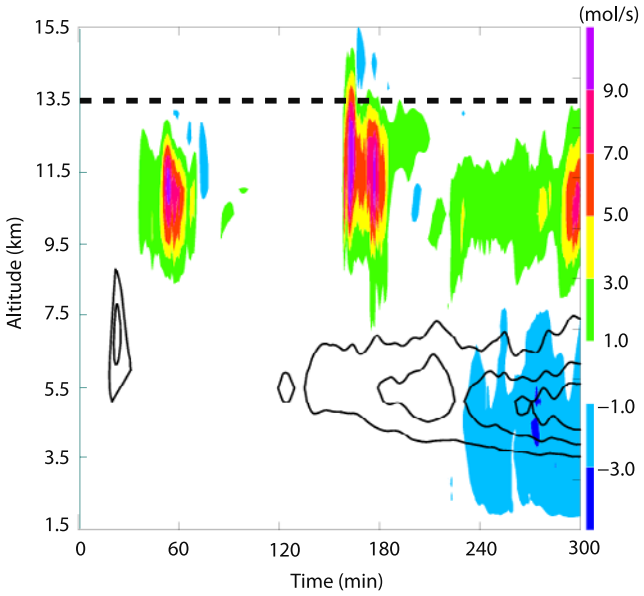

Figure 8. Time evolution of the vertical fluxes of LNO_x (colored areas in mol s^{-1}) and of the cloud droplet mixing ratio (with 1, 2 and 3 kg s^{-1} isocontours in solid lines). The dashed line indicates the tropopause height, which according to *Skamarock et al.* [2000] is at z = 13,500 m.

flux of NO_x without the LNO_x source are close to those of *Skamarock et al.* [2003]. Concerning the observed anvil flux of total NO_x during the multicellular stage, our computations are reliable to within 30%, approximately (see the additional features in Figure 9). Meso-NH tends to underestimate the anvil flux of LNO_x, which could be explained by the underestimation of the flash frequency by the model.

[25] One final point involves the estimates of flash length and of NO_x production, summarized in Table 2 for different STERAO case studies. The number of NO molecules per meter of flash is estimated with Meso-NH using (1) with P = 300 hPa which is roughly the pressure at the boundary between the two regions of opposite charge. *Stith et al.* [1999] analyzed the 9 and 10 July cases. For these two storms, they estimated NO_x production to be in the range of 2×10^{20} to 1×10^{22} molecules per meter of flash. Assuming flash lengths between 5 and 50 km, they deduced that lightning flashes might produce between 20 and 200 moles of NO_x per flash. The results of *Skamarock et al.* [2003] for the 10 July storm are based on an average flash length of 68 km from interferometric data. On the basis of 43 moles of NO_x per flash, their estimate is 1×10^{21} molecules of NO_x produced per flash. *Defer et al.* [2003] revised the total flash length of the 10 July storm down to 102,000 km. This leads to an average of 20 km per flash. The Meso-NH electrical scheme simulates a mean flash length of 30 km in accord with *Stith et al.* [1999] and in rough agreement with *Defer et al.* [2003]. The number of NO molecules per meter of flash is in the lower part of range of *Stith et al.* [1999] and is about the estimate of *Skamarock et al.* [2003]. This survey from the STERAO literature shows that Meso-NH simulates reasonably well the mean lightning flash length [*Defer et al.*, 2003] and the NO_x production per flash [*Skamarock et al.*, 2003] and always stays in the range of *Stith et al.* [1999].

5. Conclusion

[26] An explicit lightning-produced NO_x parameterization has been used for the first time to evaluate the production of NO_x by lightning in a STERAO storm. The lightning flash frequency and the total path length are key factors which are determined by the simulated electrical state of the storm. In contrast with the study of *Zhang et al.* [2003b], our model is able to simulate more than 2000 flashes and a few ppbv of NO_x per flash. Here each flash (IC or CG) is associated to a LNO_x production which is simply proportional to the flash length and to the air pressure [*Wang et al.*, 1998]. No integral constraint on the total LNO_x production at storm scale is necessary. This means that the combination of the lightning scheme of *Barthe et al.* [2005] and of the lightning length-based LNO_x production of *Wang et al.* [1998] is realistic and promising. It is deemed to also provide a better estimate of the location and timing of the LNO_x sources during five hours of simulated storm evolution.

[27] Our results show that a first large amount of LNO_x is selectively produced in the upper part of the storm, close to the updraft cores. This develops in response to subtle changes of the electrical state of individual cells, which

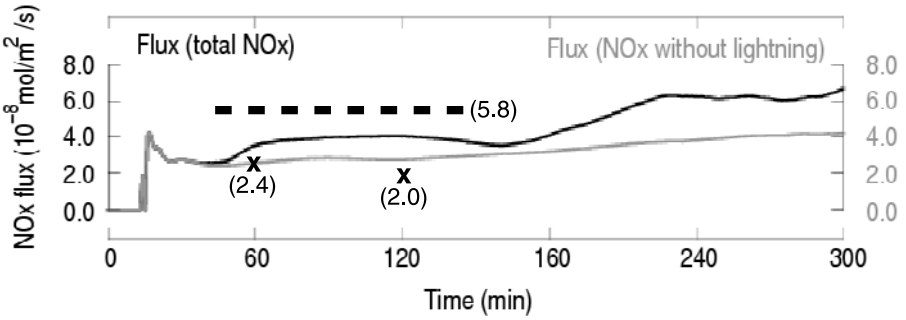

Figure 9. Time evolution of total NO_x (solid curve) and NO_x without LNO_x (shaded curve) anvil flux density. Numbers in parentheses associated with the black crosses represent simulation results from *Skamarock et al.* [2003]. The dashed line and the associated number in parentheses represent observations during the multicellular stage [*Skamarock et al.*, 2003].

Table 2. Summary of STERAO Studies With Estimations of Mean Flash Length and of NO_x Production[a]

	Mean Flash Length, km	NO Molecules per Meter of Flash	NO Moles per Flash
Stith et al. [1999]	5–50	2×10^{20} to 1×10^{22}	20–200
Skamarock et al. [2003]	68	1×10^{21}	43
Defer et al. [2003]	20	–	–
Meso-NH (this study)	30	0.73×10^{21}	36

[a]The number of NO molecules of the Meso-NH case are estimated using equation (1) with $P = 300$ hPa.

helps to trigger or to inhibit extended lightning flashes. LNO_x is then transported by the horizontal flow and diluted in the anvil. The computed LNO_x flux density in the anvil is comparable to that presented by *Skamarock et al.* [2003].

[28] As noted by *Skamarock et al.* [2003], the amount of LNO_x in the 10 July 1996 STERAO storm may not be representative of a typical storm because it was long-lived and produced numerous flashes. Therefore it would be worthwhile to apply this CRM approach to other convective events in the tropics and in the midlatitudes. This should help to improve LNO_x parameterizations in regional and global models.

Appendix A

[29] The horizontal flux density calculations are made by considering an elementary surface $[\underline{\Delta l} \times dz]$ of the anvil, normally oriented to the mean flow $\vec{U}$ with components u and v along the x and y directions, respectively (Δx and Δy are the mesh sizes). The anvil is defined column by column, between z-levels, *zbase* and *ztop*, where the ice mixing ratios are larger than a small threshold (0.01 g kg^{-1}). Defining $[NO_x]$, the local NO_x concentration and ρ, the air density, one gets

$$S(x,y) = \int_{zbase}^{ztop} \Delta l dz = \int_{zbase}^{ztop} \frac{(|u|\Delta x + |v|\Delta y)}{\sqrt{u^2+v^2}} dz,$$

$$F_h^{NO_x}(x,y) = \int_{zbase}^{ztop} \rho[NO_x]\left(\vec{U}\cdot\vec{n}\right)\Delta \mathrm{ldz} = \int_{zbase}^{ztop} \rho[NO_x](|\mathrm{u}|\Delta \mathrm{x} + |\mathrm{v}|\Delta \mathrm{y})dz.$$

$S(x, y)$ is the surface of a vertical column of the anvil across which the horizontal flux of NO_x is computed. The mean NO_x horizontal flux density across the anvil, $\langle F_h^{NO_x} \rangle$, is given by

$$\langle F_h^{NO_x} \rangle = \overline{F_h^{NO_x}(x,y)/S(x,y)}^{x,y}$$

where $\overline{()}^{x,y}$ is an horizontal average operator.

[30] **Acknowledgments.** We warmly thank Jim Dye (NCAR) for his patient review of an earlier draft and for specially redrawing the NO_x record presented in Figure 1. Discussions with Eric Defer (now at Observatoire de Paris, France) were very helpful in interpreting the lightning data of the ONERA interferometer. Mary Barth (NCAR) is acknowledged for providing us with the STERAO storm data, and Jean-Pierre Chaboureau (LA) is acknowledged for his careful review and encouragements. The manuscript was kindly proofread by Dale Durran from University of Washington during his short stay at LA. Juan Escobar and Didier Gazen (both at LA) are thanked for their assistance in running Meso-NH on the LA PC cluster.

References

Allen, D. J., and K. E. Pickering (2002), Evaluation of lightning flash rate parameterizations for use in a global chemical transport model, *J. Geophys. Res.*, *107*(D23), 4711, doi:10.1029/2002JD002066.

Altaratz, O., T. Reisin, and Z. Levin (2005), Simulation of the electrification of winter thunderclouds using the three-dimensional Regional Atmospheric Modeling System (RAMS) model: Single cloud simulations, *J. Geophys. Res.*, *110*, D20205, doi:10.1029/2004JD005616.

Barthe, C., G. Molinié, and J.-P. Pinty (2005), Description and first results of an explicit electrical scheme in a 3D cloud resolving model, *Atmos. Res.*, *76*, 95–113.

Choi, Y., Y. Wang, T. Zeng, R. V. Martin, T. P. Kurosu, and K. Chance (2005), Evidence of lightning NOx and convective transport of pollutants in satellite observations over North America, *Geophys. Res. Lett.*, *32*, L02805, doi:10.1029/2004GL021436.

Cuxart, J., P. Bougeault, and J.-L. Redelsperger (2000), A turbulence scheme for mesoscale and large-eddy simulations, *Q. J. R. Meteorol. Soc.*, *126*, 1–30.

DeCaria, A. J., K. E. Pickering, G. L. Stenchikov, J. R. Scala, J. L. Stith, J. E. Dye, B. A. Ridley, and P. Laroche (2000), A cloud-scale model study of lightning-generated NO_x in an individual thunderstorm during STERAO-A, *J. Geophys. Res.*, *105*, 11,601–11,616.

DeCaria, A. J., K. E. Pickering, G. L. Stenchikov, and L. E. Ott (2005), Lightning-generated NO_x and its impact on tropospheric ozone production: A three-dimensional modeling study of a Stratosphere-Troposphere Experiment: Radiation, Aerosols and Ozone (STERAO-A) thunderstorm, *J. Geophys. Res.*, *110*, D14303, doi:10.1029/2004JD005556.

Defer, E., P. Blanchet, C. Théry, P. Laroche, J. E. Dye, M. Venticinque, and K. L. Cummins (2001), Lightning activity for the July 10, 1996, storm during the Stratosphere-Troposphere Experiment: Radiation, Aerosol, and Ozone-A (STERAO-A) experiment, *J. Geophys. Res.*, *106*(D10), 10,151–10,172.

Defer, E., P. Laroche, J. E. Dye, and W. Skamarock (2003), Use of total lightning lengths to estimate NO_x production in a Colorado thunderstorm, paper presented at 12th International Conference on Atmospheric Electricity, June 9–13, Int. Comm. on Atmos. Electr., Versailles, France.

Dye, J. E., et al. (2000), An overview of the Stratospheric-Tropospheric Experiment: Radiation, Aerosols, and Ozone (STERAO)-Deep Convection experiment with results for the July 10, 1996 storm, *J. Geophys. Res.*, *105*, 10,023–10,045.

Fehr, T., H. Höller, and H. Huntrieser (2004), Model study on production and transport of lightning-produced NO_x in a EULINOX supercell storm, *J. Geophys. Res.*, *109*, D09102, doi:10.1029/2003JD003935.

Helsdon, J. H., Jr. (2004), Comment on "On the roles of deep convective clouds in tropospheric chemistry" by Chien Wang and Ronald G. Prinn, *J. Geophys. Res.*, *109*, D10204, doi:10.1029/2003JD001571.

Helsdon, J. H., and R. D. Farley (1987), A numerical modeling study of a Montana thunderstorm: 2. Model results versus observations involving electrical aspects, *J. Geophys. Res.*, *92*, 5661–5675.

Helsdon, J. H., G. Wu, and R. D. Farley (1992), An intracloud lightning parameterization scheme for a storm electrification model, *J. Geophys. Res.*, *97*, 5865–5884.

Huntrieser, H., H. Schlager, C. Feigl, and H. Höller (1998), Transport and production of NO_x in electrified thunderstroms: Surveys of previous studies and new observations at midlatitudes, *J. Geophys. Res.*, *103*, 28,247–28,264.

Huntrieser, H., et al. (2002), Airborne measurements of NO_x, tracer species, and small particles during the European Lightning Nitrogen Oxides Experiment, *J. Geophys. Res.*, *107*(D11), 4113, doi:10.1029/2000JD000209.

Kasemir, H. W. (1960), A contribution to the electrostatic theory of a lightning discharge, *J. Geophys. Res.*, *65*, 1873–1878.

Kasemir, H. W. (1983), Static discharge and triggered lightning, paper presented at 8th International Aerospace and Ground Conference on Lightning and Static Electricity, Natl. Interagency Coord. Group on Lightning and Static Electr., Fort Worth, Tex.

Lafore, J., et al. (1998), The Meso-NH atmospheric simulation system. Part I: Adiabatic formulation and control simulations, *Ann. Geophys.*, *16*, 90–109.

Lange, L., et al. (2001), Detection of lightning-produced NO in the midlatitude upper troposphere during STREAM 1998, *J. Geophys. Res.*, *106*, 27,777–27,785.

Lee, D. S., I. Kohler, E. Grobler, F. Rohrer, R. Sausen, L. Gallardo-Klenner, J. G. J. Olivier, F. J. Dentener, and A. F. Bouwman (1997), Estimations of global NO_x emissions and their uncertainties, *Atmos. Environ.*, *31*, 1735–1749.

MacGorman, D. R., A. A. Few, and T. L. Teer (1981), Layered lightning activity, *J. Geophys. Res.*, *86*, 9900–9910.

Mansell, E. R., D. MacGorman, C. L. Ziegler, and J. M. Straka (2002), Simulated three-dimensional branched lightning in a numerical thunderstorm model, *J. Geophys. Res.*, *107*(D9), 4075, doi:10.1029/2000JD000244.

Marshall, T. C., M. P. MacCarthy, and W. D. Rust (1995), Electric field magnitudes and lightning initiation in thunderstorms, *J. Geophys. Res.*, *100*, 7097–7103.

Meijer, E. W., P. F. J. van Velthoven, A. M. Thompson, L. Pfister, H. Schlager, P. Schulte, and H. Kelder (2000), Model calculations of the impact of NO_x from air traffic, lightning, and surface emissions, compared with measurements, *J. Geophys. Res.*, *105*, 3833–3850.

Pickering, K. E., Y. Wang, W. K. Tao, C. Price, and J.-F. Muller (1998), Vertical distributions of lightning NO_x for use in regional and global chemical transport models, *J. Geophys. Res.*, *103*, 31,203–31,216.

Price, C., and D. Rind (1992), A simple lightning parameterization for calculating global lightning distributions, *J. Geophys. Res.*, *97*, 9919–9933.

Price, C., J. Penner, and M. Prather (1997), NO_x from lightning: 1. Global distribution based on lightning physics, *J. Geophys. Res.*, *102*, 5929–5941.

Ridley, B., et al. (2004), Florida thunderstorms: A faucet of reactive nitrogen to the upper troposphere, *J. Geophys. Res.*, *109*, D17305, doi:10.1029/2004JD004769.

Ridley, B. A., K. E. Pickering, and J. E. Dye (2005), Comments on the parameterization of lightning-produced NO in global chemistry-transport models, *Atmos. Environ.*, *39*, 6184–6187.

Rison, W., R. J. Thomas, P. R. Krehbiel, T. Hamlin, and J. Harlin (1999), A GPS-based three-dimensional lightning mapping system: Initial observations in central New Mexico, *Geophys. Res. Lett.*, *26*, 3573–3576.

Rust, W. D., and D. R. MacGorman (2002), Possibly inverted-polarity electrical structures in thunderstorms during STEPS, *Geophys. Res. Lett.*, *29*(12), 1571, doi:10.1029/2001GL014303.

Skamarock, W. C., et al. (2000), Numerical simulations of the July 10 Stratospheric-Tropospheric Experiment: Radiation, Aerosol, and Ozone/Deep Convection Experiment convective system: Kinematics and transport, *J. Geophys. Res.*, *105*, 19,973–19,990.

Skamarock, W. C., J. E. Dye, E. Defer, M. C. Barth, J. L. Stith, B. A. Ridley, and K. Baumann (2003), Observational- and modeling-based budget of lightning-produced NO_x in a continental thunderstorm, *J. Geophys. Res.*, *108*(D10), 4305, doi:10.1029/2002JD002163.

Stith, J., J. Dye, B. Ridley, P. Laroche, E. Defer, K. Baumann, G. Hübler, R. Zerr, and M. Venticinque (1999), NO signatures from lightning flashes, *J. Geophys. Res.*, *104*, 16,081–16,089.

Stolzenburg, M., W. D. Rust, and T. C. Marshall (1998), Electrical structure in thunderstorm convective regions: 1. Mesoscale convective systems, *J. Geophys. Res.*, *103*, 14,059–14,078.

Takahashi, T. (1978), Riming electrification as a charge generation mechanism in thunderstorms, *J. Atmos. Sci.*, *35*, 1536–1548.

Wang, C., and R. G. Prinn (2000), On the roles of deep convective clouds in tropospheric chemistry, *J. Geophys. Res.*, *105*, 22,269–22,297.

Wang, Y. A., W. DeSilva, G. C. Goldenbaum, and R. R. Dickerson (1998), Nitric oxide production by simulated lightning: Dependence on current, energy and pressure, *J. Geophys. Res.*, *103*, 19,149–19,159.

Williams, E. R. (1989), The tripole structure of thunderstorms, *J. Geophys. Res.*, *94*, 13,151–13,167.

Zhang, X., J. H. Helsdon, and R. D. Farley (2003a), Numerical modeling of lightning-produced NO_x using an explicit lightning scheme: 1. Two-dimensional simulation as a proof of concept, *J. Geophys. Res.*, *108*(D18), 4579, doi:10.1029/2002JD003224.

Zhang, X., J. H. Helsdon, and R. D. Farley (2003b), Numerical modeling of lightning-produced NO_x using an explicit lightning scheme: 2. Three-dimensional simulation and expanded chemistry, *J. Geophys. Res.*, *108*(D18), 4580, doi:10.1029/2002JD003225.

C. Barthe, C. Mari, and J.-P. Pinty, Laboratoire d'Aérologie, Observatoire Midi-Pyrénées, 14 avenue Edouard Belin, F-31400 Toulouse, France. (barc@aero.obs-mip.fr; marc@aero.obs-mip.fr; pinjp@aero.obs-mip.fr)